CHAPTER 101

INTERACTION OF NONLINEAR WAVES WITH COASTAL STRUCTURES

J.J. Lee [1], C. Chang [2], F. Zhuang [2]

ABSTRACT

Interaction of transient nonlinear waves (modeled by solitary waves with moderate wave height) with submerged breakwater has been studied both numerically and experimentally. The emphasis is on the comparison between the numerical solution and the laboratory experiments on the wave transformation and the water particle velocity of the induced flow field.

For the numerical analysis, the Boundary Element Method (BEM) has been used for analyzing the wave field induced by the coastal structure. For the laboratory experiments the wave profiles are obtained by resistance type wave gauge; the two dimensional water particle velocities are obtained by a four-beam Laser Doppler Velocimeter (LDV) equipped with frequency shifting and with a fiber optics system. The LDV measurements are directed to obtain the detail of the wave kinematic properties important for ascertaining the dynamics of the modified wave field in the vicinity of the submerged breakwater. This serves as a critical check for the validity of the numerical computations.

Results of the numerical model have been found to compare well with the experimental data for the conditions studied in both the wave profiles and the water particle velocities beneath the waves as they interact with the breakwater.

[1]Jiin-Jen Lee, Member, ASCE; Professor of Civil Engineering, Department of Civil Engineering, University of Southern California, Los Angeles, CA 90089-2531

[2]Chun Chang & Fei Zhuang, Graduate Research Assistants, Department of Civil Engineering, University of Southern California, Los Angeles, CA 90089-2531

1 Numerical Analysis

For the numerical analysis, the problem is formulated as a two-dimensional boundary value problems. The fluid in the solution domain is assumed to be incompressible and the flow irrotational, the viscous force is neglected. Potential theory is used for such flow condition and the Laplace's equation is obtained as the governing equation:

$$\nabla^2\phi(\mathbf{x},t) = 0 \qquad \mathbf{x} \in \Omega(t). \tag{1}$$

The solution to the Laplace's equation is expressed as a boundary integral using the free space Green's function $G(\mathbf{x}_i,\mathbf{x}_j) = -\frac{1}{2\pi}\log|\mathbf{x}_i-\mathbf{x}_j|$ and Green's theorem:

$$\alpha(\mathbf{x}_i)\phi(\mathbf{x}_i) = \int_{\Gamma(\mathbf{x})}\left[\frac{\partial\phi}{\partial n}G(\mathbf{x},\mathbf{x}_i) - \phi(\mathbf{x})\frac{\partial G(\mathbf{x},\mathbf{x}_i)}{\partial n}\right]d\Gamma(\mathbf{x}) \tag{2}$$

where $\mathbf{x}_i$ and $\mathbf{x}$ are position vectors for position on the boundary ($\mathbf{x}_i$ can also be any where within the domain), $\Gamma(\mathbf{x})$ is the boundary of the fluid domain Ω, $\mathbf{n}$ the unit outward normal vector and $\alpha(\mathbf{x}_i)$ a geometric coefficient.

The kinematic and the fully nonlinear dynamic free surface conditions are considered, i.e., on the free surface Γ_s, ϕ satisfies the following kinematic and dynamic boundary conditions:

$$\frac{D\mathbf{r}}{Dt} = (\frac{\partial}{\partial t} + \mathbf{u}\cdot\nabla)\mathbf{r} = \mathbf{u} = \nabla\phi \tag{3}$$

$$\frac{D\phi}{Dt} = -gy + \frac{1}{2}|\nabla\phi|^2 - \frac{p_a - p_o}{\rho} \tag{4}$$

with $\mathbf{r}$ the position vector of a fluid particle at the free surface, g the acceleration due to gravity, y the vertical coordinate, p_a the pressure at the surface, p_o a reference pressure and ρ the fluid density.

The method used to update both the new position of the free surface and the potential function ϕ on the free surface at the next time step was first suggested by Dold and Peregrine (1986). Similar procedure was also used by Grilli, Skourup & Svendsen (1989). Based on the Taylor expansion in a Lagrangian formulation (following a fluid particle on the surface), the explicit expressions for the position vector $\mathbf{r}(t+\Delta t)$ and the potential function $\phi(t+\Delta t)$ can be expressed as an infinite series as follows:

$$\mathbf{r}(t+\Delta t) = \mathbf{r}(t) + \sum_{k=1}^{n}\frac{(\Delta t)^k}{k!}\frac{D^k\mathbf{r}(t)}{Dt^k} + O[(\Delta t)^{n+1}] \tag{5}$$

$$\phi(\mathbf{r}(t+\Delta t),t+\Delta t) = \phi(\mathbf{r}(t),t) + \sum_{k=1}^{n}\frac{(\Delta t)^k}{k!}\frac{D^k\phi(\mathbf{r}(t),t)}{Dt^k} + O[(\Delta t)^{n+1}]. \tag{6}$$

The terms containing the material derivatives of $\mathbf{r}$ and ϕ in the above two equations are determined by first expressing them in terms of the potential function ϕ and its time and spatial derivatives $(\frac{\partial\phi}{\partial n}, \frac{\partial^2\phi}{\partial t\partial n}, \cdots)$ and then solve the time and spatial derivatives by solving successions of Laplace's problems for the velocity potential ϕ and its time derivatives. Each solution provides the nonlinear free surface boundary conditions for the next one. This is applicable because the Laplace's equation is indeed valid for all the time derivatives of ϕ. The repeated solution of the Laplace's equation is actually quite simple after the coefficient matrix of the boundary element method has been formed and decomposed into an upper and a lower diagonal matrix. This is so because the coefficient matrix is only a function of the geometry and remain unchanged throughout the repeated solution process.

The Boundary Integral Equation is solved by using the so called Boundary Element Method which discretize the boundary into a finite number of elements. The boundary integration is performed on each element for a given $\mathbf{x}_i$, $i = 1, 2, \ldots, N$,

$$\alpha(\mathbf{x}_i)u(\mathbf{x}_i) = \sum_{k=1}^{N}\left\{\int_{\Gamma_k}[\overline{\frac{\partial u}{\partial n}}G - u\frac{\partial G}{\partial n}]d\Gamma + \int_{\Gamma_k}[\frac{\partial u}{\partial n}G - \overline{u}\frac{\partial G}{\partial n}]d\Gamma\right\}. \quad (7)$$

This produces a system of N linear algebraic equations for N unknowns. The integral equation is solved twice in the present study for both ϕ and $\partial\phi/\partial t$. This gives a second order accuracy in the time marching scheme.

Interior solutions at the interior point x_j can be obtained using

$$2\pi\phi(x_j) = \int_\Gamma[\phi(x_i)\frac{\partial}{\partial n}(\ln r) - \ln r\frac{\partial}{\partial n}\phi(x_i)]ds \quad (8)$$

when all the potential values and normal potential derivatives on the boundary (for all x_i) are known. Normally the value of the potential function inside the domain is not as important as its derivatives with respect to x and y because these values represent the velocity components at the interior points. The calculation of these velocity components can be performed by making direct derivatives of Equation 8 with respect to x and y, respectively,

$$2\pi\frac{\partial}{\partial x}\phi(x_j) = \int_\Gamma[\phi(x_i)\frac{\partial}{\partial x}(\frac{1}{r}\frac{\partial r}{\partial n}) - \frac{\partial}{\partial x}(\ln r)\frac{\partial}{\partial n}\phi(x_i)]ds \quad (9)$$

$$2\pi\frac{\partial}{\partial y}\phi(x_j) = \int_\Gamma[\phi(x_i)\frac{\partial}{\partial y}(\frac{1}{r}\frac{\partial r}{\partial n}) - \frac{\partial}{\partial y}(\ln r)\frac{\partial}{\partial n}\phi(x_i)]ds. \quad (10)$$

Only ϕ at the interior point x_j is differentiated since that is where the derivatives are wanted. From Equation 9 & 10 it is seen that the values of ϕ, $\frac{\partial\phi}{\partial n}$ inside the integral are those on the boundary and they are not involved in the differentiation of the function.

2 Experimental equipment and experimental procedures

Experiments involving propagation of solitary waves over various submerged breakwater configurations are conducted in a wave tank 15.2 meter long, 39.4 centimeter wide, and 61 centimeter deep. The side-walls of the wave tank are made of glass and offer excellent transparency for laser beams. A programmable piston type wave generator is installed at one end of the tank and a sloping beach is installed at the other end of the wave tank.

Two different breakwater configurations are used in the experiment. The first breakwater is 45 inch wide, 4.5 inch high and is made of plywood. The second breakwater is of one third in width with the same height and is made of lucite. The breakwater is sunk and fixed to the bottom of the wave tank by adding lead weight.

The wave generating device is a piston type wave generator. It is powered by a hydraulic piston whose motion is controlled by a personal computer. The computer determines a voltage time history which defines the trajectory of the wave plate through a hydraulic-servo system. The wave generation program used by the computer allows motions of the wave machine to be prescribed for generating small amplitude periodic waves, finite amplitude periodic waves, and solitary waves.

Tap water is used to fill the wave tank to the desired depth. The depth is measured using a point gage which is mounted to a movable carriage traveling on a rail system installed at the top of both side walls of the wave tank. Resistance type wave gages are used to measure water surface elevations as a function of time. Three wave gages are installed at desired locations to make simultaneous wave profile measurements. The wave gages are connected to a Sanborn four channel oscillograph recorder which records the measurements on an oscillograph paper.

The water particle velocities are measured using a portable four-beam, two-component, fiber optic Laser Doppler Velocimeter (LDV) manufactured by TSI, Inc.. The LDV system used in the experiment consists of a 100 mW argon-ion laser, transmitting and receiving optics, a fiberoptic probe, frequency shifting and signal processing instruments. A multicolor beam separator separates the incident laser beam into four beams, two blue beams and two green beams. The four laser beams are focused into one point within the flow field to form a two-component system. Figure 1 provides a flow chart of the LDV system used for the present experiment. Two photomultipliers convert optical signals into electric signals. Two frequency shifters help attain accurate flow measurements in applications where high turbulence or flow

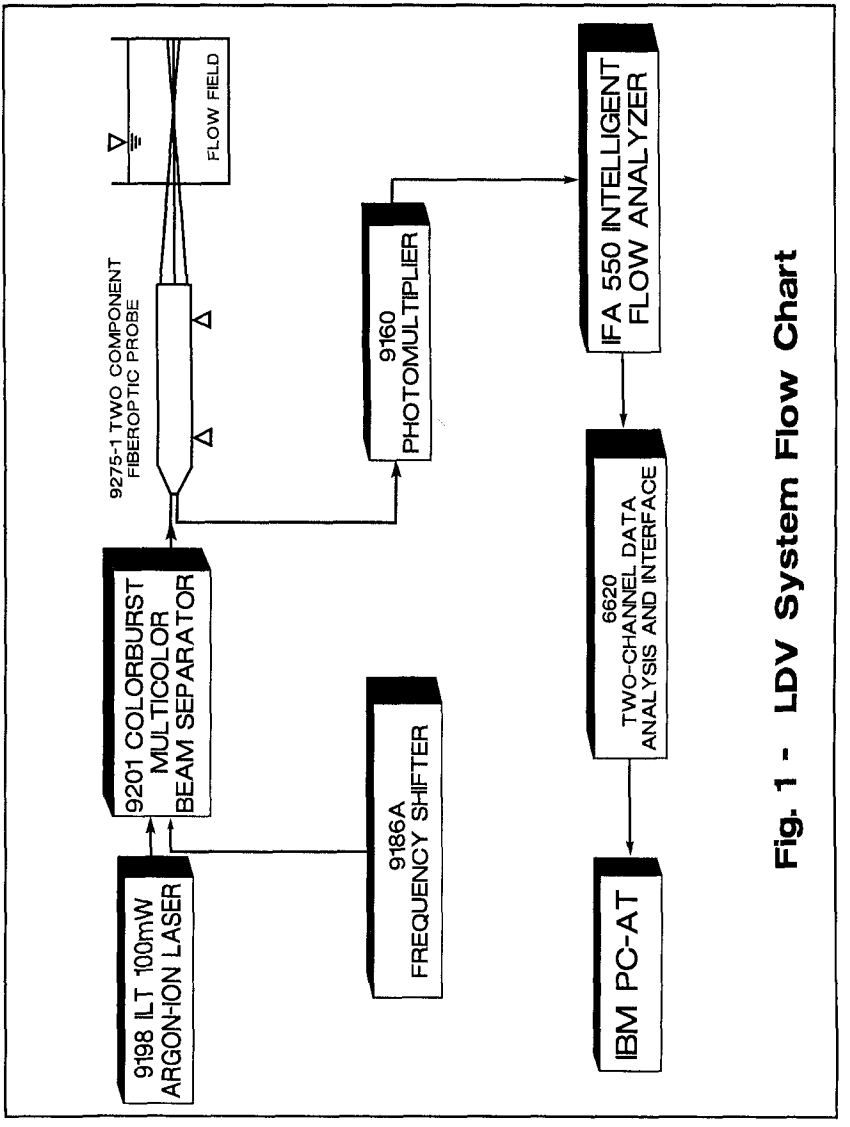

Fig. 1 - LDV System Flow Chart

reversals are anticipated. A fiberoptic probe which features focusing and receiving optics in one compact unit offer considerable ease for setting up the LDV system. Two IFA550 signal analysis systems are used for signal analysis. This is done by using a personal computer which manages the LDV measurements, stores velocity measurements, and displays the velocity-time history on the monitor. The whole LDV system is installed in a room close to the wave tank. When velocity measurements are needed, only the portable fiberoptic probe is moved to the measuring station and is mounted to a traversing mechanism which offers three dimensional positioning of the measuring point. Seeding is one of the key elements affecting the performance of the LDV measurements. Seeding particles must be small enough to move with the flow yet large enough to scatter sufficient light for ideal signal quality. Titanium Dioxide powder (TiO_2) is used in the experiment and is proved to be a good seeding agent for water in the wave tank used for the present experiments.

3 Presentation and Discussion of Results

Figure 2 shows the wave profiles obtained from the numerical model at different time steps as the incident solitary wave propagates over a submerged breakwater which is at one-half of the water depth. The wave height/water depth ratio is 0.2, still water depth is 9 inches and the breakwater width is ten times the breakwater height. It should be noted that the vertical scale in Figure 2 is greatly distorted for easy visualization of the wave profiles. From Figure 2 it is seen that the frontal slope of the solitary wave is steepened when the propagating wave approaches the shallower water depth region. It is evident that the submerged breakwater acts to breakup the solitary wave with significant oscillatory tails.

Figure 3 shows the wave profiles computed at three locations: five water depth upstream, five water depth downstream, and on the top of the breakwater. The wave profiles computed from the present numerical model are compared with the wave profiles recorded from the present experiments. It should be noted that the wave profiles shown in Figure 2 are for the Lagrangian system and the time history of the computed wave profile shown in Figure 3 has been converted to the Eulerian reference system so that the computed wave profiles can be compared with the experimental wave profile directly. A comparison of the numerical results and the experimental wave profiles at the three locations shown in Figure 3 clearly demonstrate that the numerical model predicts the wave profile well. It is interesting to note that the peak amplitude of the transmitted solitary wave at the location five water depth downstream of the breakwater is actually larger than the amplitude of

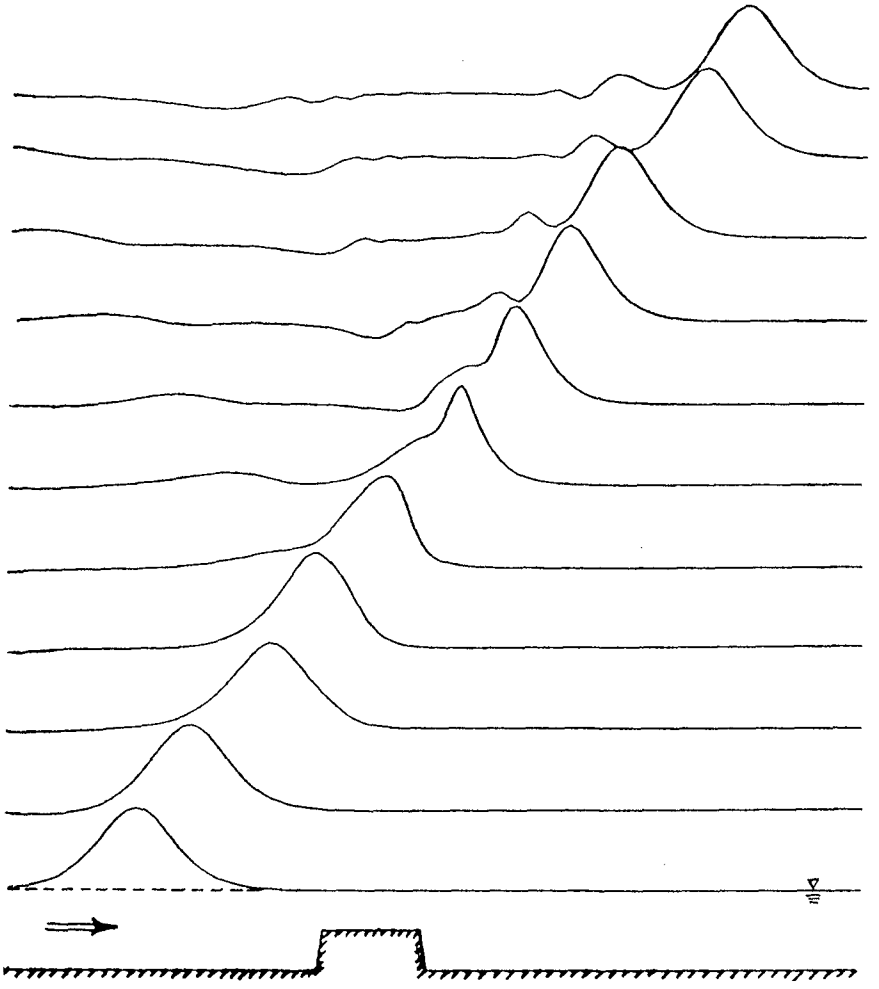

Figure 2: Transformation of solitary wave over submerged breakwater

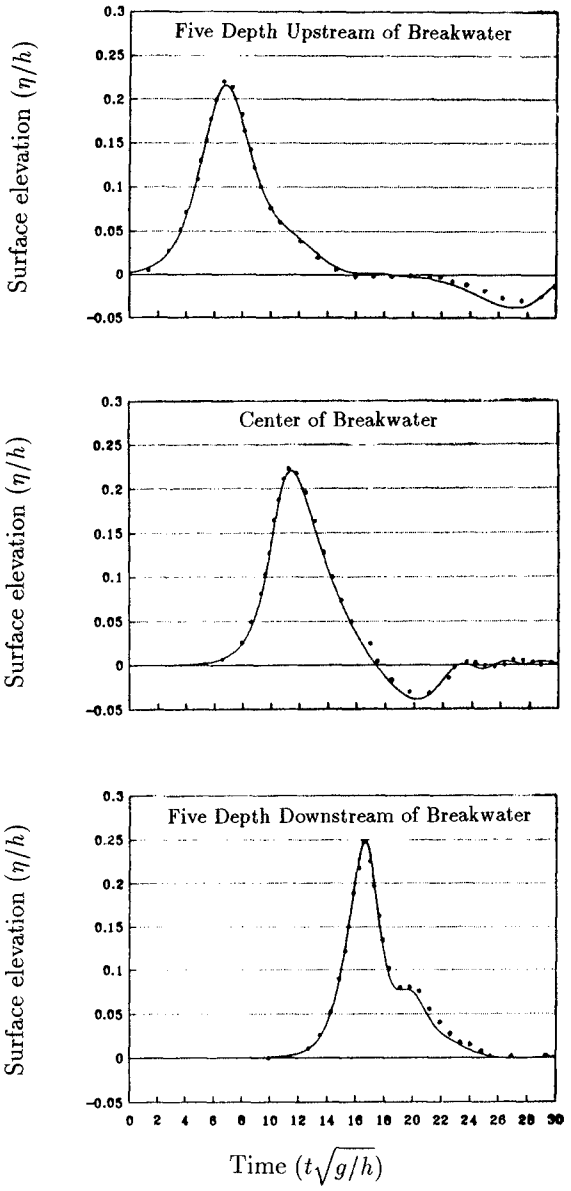

Figure 3: Comparison of wave profiles at three different locations (— present theory, $\cdots$ experiment)

the incident solitary wave before interacting with the breakwater. The shape of wave profile is different at the three locations showing the different degree of interaction with respect to transmission, reflection, and the varying water depths effect.

Figure 4 shows the numerical model and the experimental data on the horizontal and vertical water particle velocity at the same three horizontal locations and at 0.1 water depth below the still water level. In each of the three figures shown the horizontal velocities are significantly larger than the vertical velocities. Comparing the numerical and experimental results one can see that the agreement is quite good even though there is some scattering when the velocity is very small. The good agreement between the theory and experiment for the two components of the water particle velocities provides another critical check of the reliability of the numerical model.

Experiments for different water depths resulting in several cases for different relative submergence of the breakwaters have been conducted. LDV measurements for horizontal and vertical components of the water particle velocities have also been conducted at many different locations. However, space limitation does not permit presentation of these additional results.

Experiments have also been conducted for the case of breakwater crest height exactly at the still water level. Thus the incident solitary wave will travel across the top of the breakwater as if wave is traveling at zero water depth. A sketch of this series of experiments is shown in Figure 5. Wave profiles are measured at three stations: one at 10 water depth upstream of the breakwater (45" upstream), another at 3.33 water depth downstream of the breakwater (15" downstream) and the third station at 10 water depth downstream of the center of the breakwater (45" downstream).

The incident solitary wave height is $H/h = 0.2$. The measured wave profiles are presented in Figures 6-8. The ordinates of these three figures represent the wave height (H) normalized with respect to the water depth (h). The abscissa represents the real time in seconds.

From Figure 6 it is clear that the majority of the first wave represents the incident solitary wave and the second wave represents the reflected wave from the upstream edge of the breakwater. The shape of the reflected wave is quite similar to the solitary wave also. The wave profile shown in Figure 7 represents the transmitted wave profile at 15" downstream after the solitary wave has traveled above the breakwater crest region (at zero water depth). It shows that the primary wave is followed by a series of oscillatory tails. These oscillatory wave trains have been reformed into more regular oscillatory waves as they traveled further downstream as evidenced in the wave profile presented in Figure 8. It is interesting to observe the physical nature of the transmitted wave as it travels above the breakwater crest at

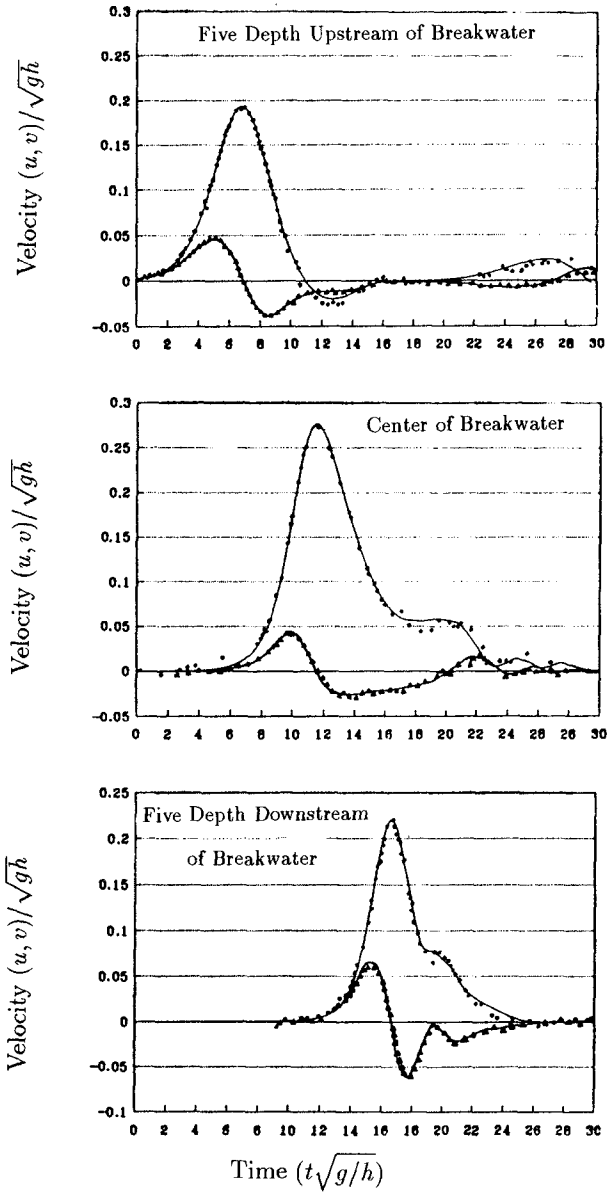

Figure 4: Comparison of water particle velocities at three different locations (— present theory; $\cdots$ experiment, u component; ▲▲▲experiment, v component)

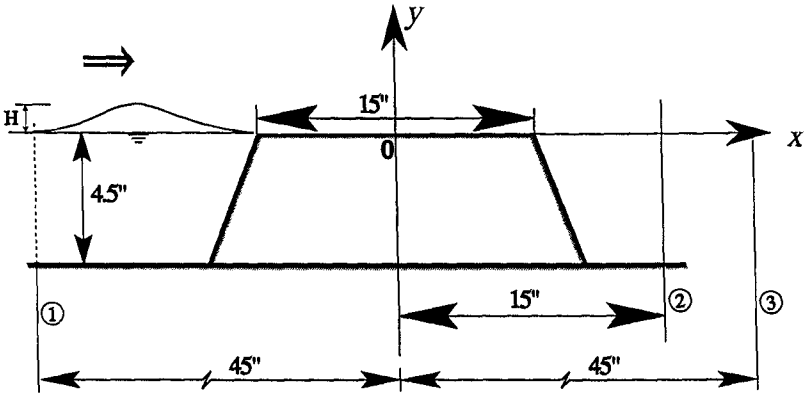

Figure 5
Sketch of an experimental set up showing the breakwater height, still water depth and locations of three wave profile measurement stations (not to scale)

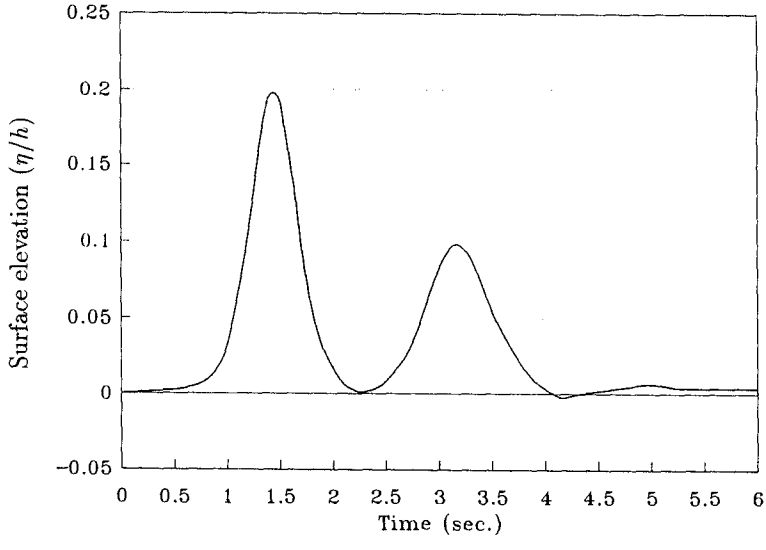

Figure 6: Wave record at 45" upstream of the center of breakwater (station 1)

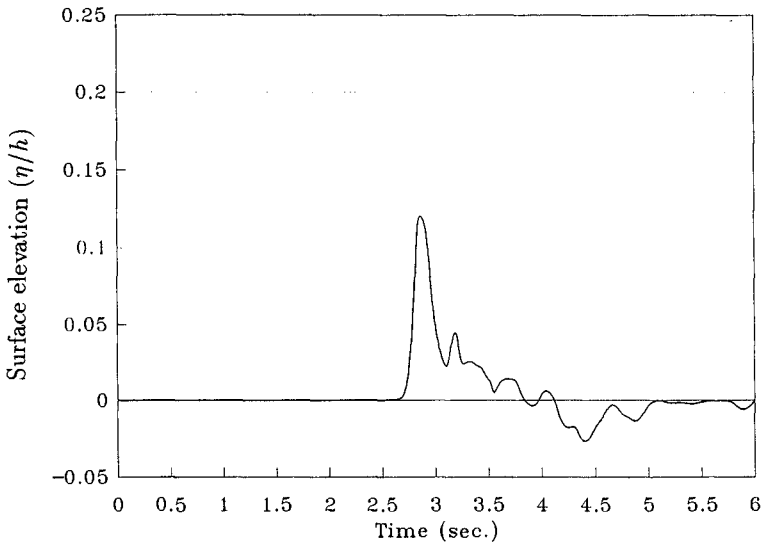

Figure 7: Wave record at 15" downstream of the center of breakwater (station 2)

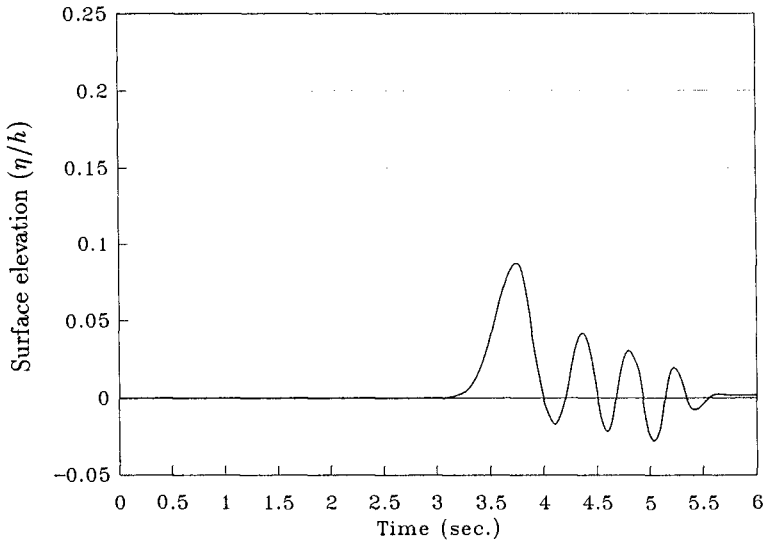

Figure 8: Wave record at 45" downstream of the center of breakwater (station 3)

zero depth. The jet like water mass is translated into the shoreward region of the breakwater. This water mass which is above the still water level then plunge into the shoreward region by the continuous effect of the gravity forces causing the water mass in the shoreward region to exhibit significant undulations. Velocity measurements in this region have also been performed but due to space limitation they are not presented herein. Comparing the wave profiles shown in Figure 6, 7, and 8, it is clear that the breakwater serves to break up the incident wave resulting in significant higher frequency wave components in the shoreward region. This physical phenomenon is significant for the assessment of basin response of the shoreward coastal region.

4 Conclusions

The interaction of solitary wave with submerged breakwater has been studied both experimentally and numerically using a boundary element method. For incident solitary wave with moderate wave height and when the breakwater is deeply submerged the numerical results have been compared with the experimental data. It is shown that the agreement between the numerical results and the experimental data has been excellent. The comparison was performed in terms of the wave profiles at various stations and the horizontal and vertical components of the water particle velocities in the vicinity of the breakwater. The LDV measurements of particle velocities are shown to be effective in resolving the velocity time history.

A series of experimental data is also presented for solitary wave interacting with the breakwater which has the same height as the still water depth. Only the experimental data is available for this aspect of the study. Since the incident wave actually travels in a certain region of zero water depth before propagating toward the shoreward region, the present numerical method would not be able to simulate this flow condition. The experimental data show that a series of higher frequency oscillatory tails is generated in the shoreward region. This transmitted wave is reformed to become a series of well defined oscillatory wave as they propagate further away from the breakwater.

5 Acknowledgment

The authors are grateful for the generosity of Dr. Fredric Raichlen for permitting them to conduct the experiments at Caltech's W.M. Keck Laboratory of Hydraulics and Water Resources. The LDV system used in this study was partially supported by an NSF grant to USC under grant No. 8906898.

Financial support from the USC Foundation for Cross-Connection Control and Hydraulic Research for this study is gratefully acknowledged.

6 Bibliography

[1] Dold, J.W. & Peregrine, D.H. (1986) "An Efficient Boundary Integral Method for Steep Unsteady Water Waves." *Numerical Methods for Fluid Dynamics II* (ed. K.W. Morton & M.J. Baines), pp. 671-679. Clarendon Press, Oxford.

[2] Grilli, S., Skourup, J. and Svendsen, I.A. (1989) "An Efficient Boundary Element Method for Nonlinear Water Waves." *Engineering Analysis with Boundary Elements,* 6(2), 97-107.